Taming the emerging beams after the split of optical vortex solitons in a saturable medium

Albert S. Reyna* and Cid B. de Araújo
Departamento de Física, Universidade Federal de Pernambuco, 50670-901, Recife, Pernambuco, Brazil
(Received 10 August 2015; revised manuscript received 24 December 2015; published 22 January 2016)

Control of the emerging beams obtained from the spontaneous splitting of an optical vortex soliton (OVS) due to the azimuthal modulation instability is demonstrated. The procedure adopted consisted of adding a *control Gaussian beam*, propagating collinearly with the OVS, and adjusting the beams' relative positions, radius, and intensities. Rotation of the emerging beams in the transverse plane and energy transfer between them were obtained using a *control beam* with smaller intensity than the vortex beam. The numerical simulations based on a modified nonlinear Schrödinger equation, including saturable nonlinearity and three-photon absorption, are in excellent agreement with the experimental results.

DOI: 10.1103/PhysRevA.93.013843

I. INTRODUCTION

The control of light by light is one fascinating process in nonlinear (NL) optics with important applications in high-speed optical processing and telecommunications [1]. Usually the all-optical control of a laser beam is obtained using an intense laser which couples with the weaker beam through cross-phase modulation (XPM) inducing polarization rotation and/or light bending [2]. Nowadays all-optical devices and prototypes can be operated with basis on the XPM allowing signal processing with high bit rates [3]. In this context, temporal and spatial solitons have attracted great attention because the invariance of their shape is an important feature in long-distance data transmission where solitons may play the role of information bits [4,5].

Bright spatial solitons are self-trapped optical beams that propagate in focusing Kerr media, due to a balance between diffraction and NL interaction [2]. The stable propagation of spatial solitons was first observed in waveguides with dominant self-focusing (SF) nonlinearity [6]. However, for light propagating in three-dimensional media the SF does not assure stable propagation of spatial solitons and catastrophic collapse is observed [7]. Nevertheless, theoretical studies [8] indicated that contributions from high-order susceptibilities may prevent the beam collapse stabilizing the solitons' propagation. Experimental demonstrations were recently reported for systems having cubic-quintic [9] and quintic-septimal [10] local nonlinearities.

On the other hand, optical vortex solitons (OVSs) show stable propagation for cubic self-defocusing media [11]. These helical beams, characterized by a phase singularity and zero amplitude at the vortex pivot, carry a nonzero orbital angular momentum (OAM) described by the phase factor $\exp(im\theta)$, where θ is the azimuthal coordinate with respect to the beam axis and m is the topological charge [12]. Experimental observations of OVSs in defocusing media were reported in [13].

Both types of solitons, bright and vortex, have large potential for applications in many areas that include optical data storage, transmission, and data processing [11].

Nevertheless, the propagation of OVSs in SF media is unstable [14–16]. In particular, it is known that in SF nondissipative media, OVSs are subject to spontaneous azimuthal symmetry breaking due to the spatial modulation instability (SMI) [14]. As a consequence the OVS is split into bright fragments, which have characteristics of fundamental solitons; the number of fragments is equal to twice the topological charge of the OVS and the observation of this phenomenon was reported in a cubic SF medium [16]. Although there are several theoretical works aimed at identifying suitable conditions for stable propagation of OVSs in SF media [17], there are few experimental results showing a robust OVS propagation in such media. The first experiments of stable propagation of discrete OVSs were reported using external potentials induced by photonic lattices [18]. Recently, different species of solitons, including OVS, were reported in a rarefied gas composed of three-level atoms with single-photon resonant nonlinearity, in a four-wave mixing (FWM) process [19]. More recently, the stable propagation of a self-trapped vortex beam in a SF material with local nonlinearity was reported in experiments with liquid carbon disulfide (CS_2) [20]. These experiments showed that an OVS with $m = 1$ and appropriate field amplitudes can be *azimuthally stable* due to the combination of saturation of the refractive nonlinearity and three-photon absorption (3PA). At high intensities, the OVS spontaneously split into two bright fragments, which move along the tangent of the initial ring-type beam profile due to OAM conservation. Although many studies analyzing the splitting of OVS were published [21], no experimental study showing a way to manage the emerging beams, via all-optical control, was published.

In this paper, we report two schemes for controlling the relative azimuthal position and energy transfer (ET) between the emerging beams after the splitting of an OVS propagating in CS_2. The superposition of copropagating Gaussian and vortex beams allowed the control of the fragments producing an angular rotation in the transverse plane that may reach $\approx 90°$ by adjusting the Gaussian beam intensity. Additionally, ET between the fragments, with efficiency up to 92%, is observed by varying the size and the relative positions of the vortex and Gaussian beams' axis. The experimental results were reproduced by numerical simulation considering the saturation of the NL refractive index and the 3PA coefficient that were previously measured for CS_2 [22]. It is important to notice

*Corresponding author: areynao@yahoo.com.br

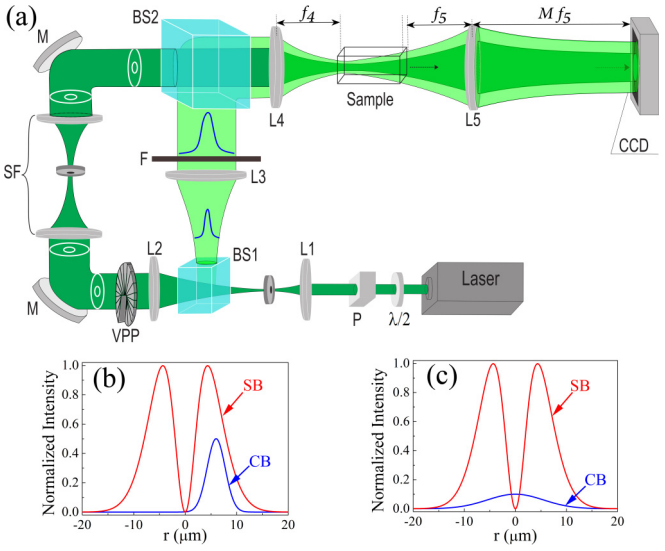

FIG. 1. (a) Schematics of the experimental setup: polarizer (P); telescopes (L1-L2 and L1-L3); vortex phase plate (VPP); mirror (M); spatial filter (SF); beam splitters (BS1 and BS2); neutral density filter (F); spherical lenses with $f_4 = 50$ mm (L4) and $f_5 = 50$ mm (L5). The CCD camera records the transverse beam spatial profile with magnification M. Transverse beam profiles at the cell's entry face used for the experimental schemes: A (b) and B (c).

that the procedure presented here is general enough to be successfully applied for other saturable media.

II. EXPERIMENTAL DETAILS

The experimental setup used is sketched in Fig. 1(a). The second-harmonic beam at 532 nm, obtained from a Nd:YAG laser (80 ps, 10 Hz, 1064 nm), with the maximum pulse energy of 10 μJ, was split into two beams using a 50:50 beam splitter (BS1). The variation of the total beam power was made using a $\lambda/2$ plate followed by a Glan prism which assures the linear polarization of the beam. Two telescopes, formed by lenses L1-L2 and L1-L3, were used to adjust the transverse beams' dimensions. The beam transmitted by the BS1 passes through a phase plate (VPP) which produces a vortex beam with $m = 1$ [the *signal beam* (SB) with intensity I_S]. A spatial filter, located after the VPP, was used to eliminate high-order diffracted light. The reflected beam by BS1 with Gaussian profile was the *control beam* (CB) with intensity I_C. This beam was collimated by lens L3, which allows adjustment of its diameter. Neutral density filters were used to vary I_C maintaining constant the beams' polarization. The SB and CB were combined using a beam splitter (BS2) and focused by a 5-cm-focal-distance lens (L4) on the input face of a 10-mm-long quartz cell filled by CS_2. The transverse beams' profiles were imaged on a charge-coupled device (CCD) camera aligned with the beam-propagation direction. The lens L5 was used to obtain the beam's image at the output face of the cell with magnification $M = 4$. Single-pulse images were captured by triggering the CCD, using a digital delay and pulse generator (DDPG), which was triggered by the Nd:YAG laser pulses, at 10 Hz, avoiding contributions of slow NL response due to thermal effects. The SB at the input face (positioned in the focal plane of the lens L4) consists of a Gaussian background, with beam waist of 11 μm, and the vortex core with radius of 3 μm. Under these conditions and for $8\ \mathrm{GW/cm^2} \leqslant I_s \leqslant 10\ \mathrm{GW/cm^2}$ a self-trapped vortex beam is formed and propagates along ~3 mm as reported in [20]. For $I_s > 10\ \mathrm{GW/cm^2}$, the SMI produces distortions in the transverse beam profile, which gradually increase up to splitting of the OVS. At 3 mm from the entrance face of the cell, the OVS is split into two bright fragments for $I_s \geqslant 18\ \mathrm{GW/cm^2}$.

III. RESULTS AND DISCUSSION

In order to control the azimuthal positions and relative intensities of the OVS fragments, two experimental schemes (A and B) were implemented varying the radius, position, and intensity of the CB with respect to the SB. Scheme A consisted of the collinear propagation of the two beams with the CB located on the side of the vortex around the core, as shown in Fig. 1(b). The CB radius is 3.5 μm. In scheme B, the SB and CB have the same transverse dimensions (the CB and vortex beam radii are of 11 μm) and their axes are coincident, as indicated in Fig. 1(c). The maximum ratio I_C/I_S used was of 0.5 and 0.1 in scheme A and scheme B, respectively. In both cases, the signal and control beams were overlapped spatially and temporally inside the sample.

Figure 2 shows images of the OVS fragments at the exit face of the cell corresponding to scheme A. Figure 2(a) shows the two emerging beams when $I_s = 18\ \mathrm{GW/cm^2}$, in the absence of the CB. The two fragments, resulting from the splitting of a single vortex beam with approximately uniform field background, have equal shape, size, and intensity [16,20,21]. Figures 2(b)–2(h) show the rotation of the fragments, in the transverse plane, for $0.5\ \mathrm{GW/cm^2} \leqslant I_C \leqslant 10\ \mathrm{GW/cm^2}$. The initial angle, $\varphi_0 = \pi/22$, between the vertical direction and the line along the fragments, in the absence of the CB, depends on the phase-plate position and the samples' nonlinearity [21,23]. By rotating the phase plate in a plane transverse to the beams' axis we observed changes of φ_0 but in the experiments described here the VPP is kept fixed. The maximum rotation angle induced by the CB, $\varphi \approx \varphi_0 + \pi/2$, was obtained for $I_C = 10\ \mathrm{GW/cm^2}$ and $I_S = 18\ \mathrm{GW/cm^2}$. The results suggest the possibility for operation of an optical switch, where the emerging beams obtained from the split of an OVS are controlled by a CB with smaller intensity than the SB intensity. It is known that CS_2 has two response times: an ultrafast one (<50 fs) and a fast one of ~2 ps [24]. However, in our case, the NL response of CS_2 is limited by the pulse duration of the incident beam, 80 ps [25]. Thereby, the modulation is as fast as the duration of the pulse.

The rotation of the fragments was investigated by placing the CB in different azimuthal positions around the vortex core and the largest rotation angle was obtained when the CB was located approximately at the bottom of the vortex on the line corresponding to $\varphi_0 = \pi/22$.

Figure 3 presents the spatial profiles of the fragments at the exit face of the cell following scheme B, for $I_S = 18\ \mathrm{GW/cm^2}$. In the absence of the CB, the two fragments have identical characteristics, as shown in Fig. 2(a). Figure 3(a) shows ET of ≈10% between the two fragments when $I_C = 0.3\ \mathrm{GW/cm^2}$. The ET was controlled by varying I_C reaching a maximum

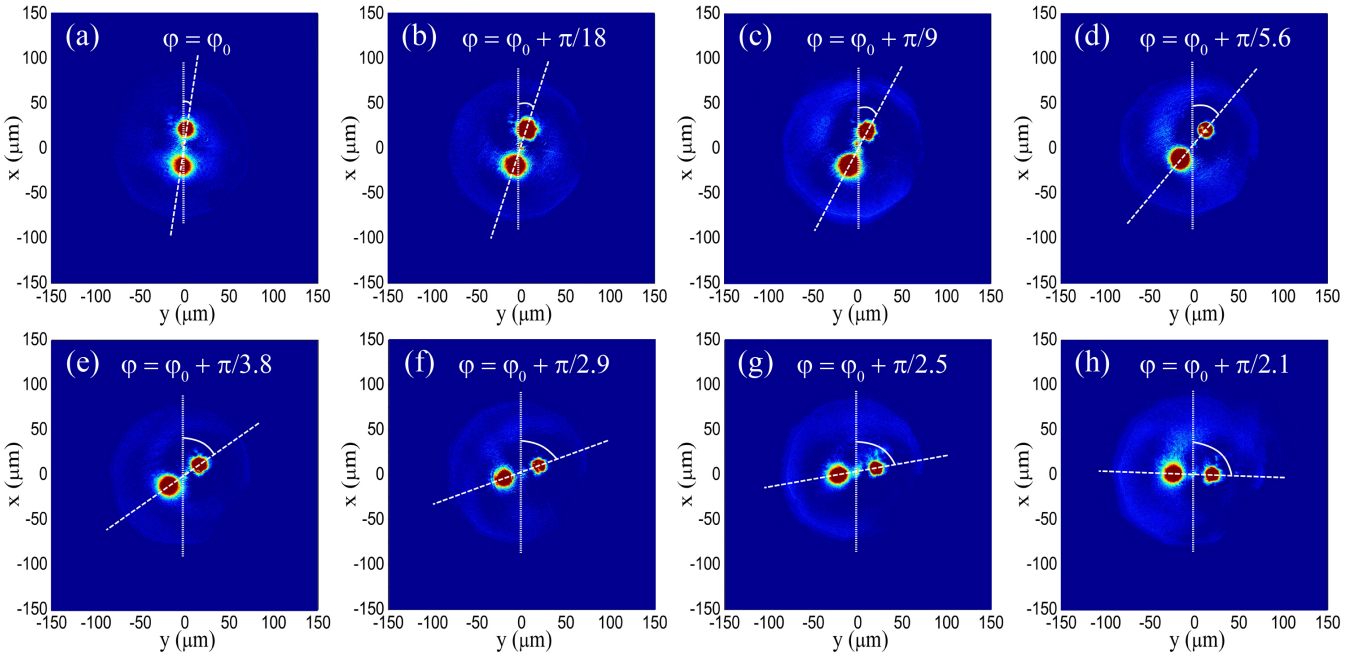

FIG. 2. Experimental images of the emerging beam's profiles at the output face of the cell obtained using scheme A. Vortex beam intensity: 18 GW/cm^2. Gaussian beam intensity (in GW/cm^2): (a) 0, (b) 0.5, (c) 1, (d) 3, (e) 5, (f) 7, (g) 9, and (h) 10. Cell length: 10 mm and $\varphi_0 = \pi/22$.

efficiency of 92% for $I_C = 2$ GW/cm^2 as shown in Fig. 3(d). In Figs. 3(a)–3(d), the color scale, which represents the intensity in the transverse plane, was normalized with respect to its maximum value in each case but the total power was conserved, in all cases. The white dashed lines (pink cross) correspond to the initial (final) position of the vortex core, in the absence (presence) of CB.

In order to understand the results of Figs. 2 and 3 we recall that the vortex beam propagation is very sensitive to the presence of external perturbations. For the I_S used, in the absence of CB, the splitting of the vortex is due to the SMI effect, as mentioned above. In the present experiments, the SMI is enhanced by the presence of the CB that induces changes in samples' refractive index in the region where the CB and SB overlap. In scheme A the CB is an off-axis perturbation for the SB. Then, the refractive index induced in the region illuminated by the CB is larger because the CS_2 is a SF medium. Thus, the bright fragments formed after the splitting of the OVS suffer changes in their rotation, which alter its final relative position, when they pass through the region where the refractive index is larger. Then, the largest rotation angle is obtained when the CB is placed closer to the position of one of the fragments, just after the split of the OVS. On the other hand, in scheme B, the CB field affects the whole area of the SB. The superposition of the Gaussian and vortex beams provides a coherent field which induces a displacement of the vortex core in the radial direction that increases with the propagation distance, incident intensity, and nonlinearity of the medium [26]. Nonuniformity in the intensity profile and asymmetries in the spatial shape of the CB contribute for enhancement of the vortex core displacement [27]. Therefore, the SB splitting is affected by the azimuthal asymmetry caused by the displacement of the vortex core. Then, the two emerging beams have different size and shape, and one of them, which has higher energy, is located in the opposite direction to the displacement direction of the vortex core. The intensity ratio

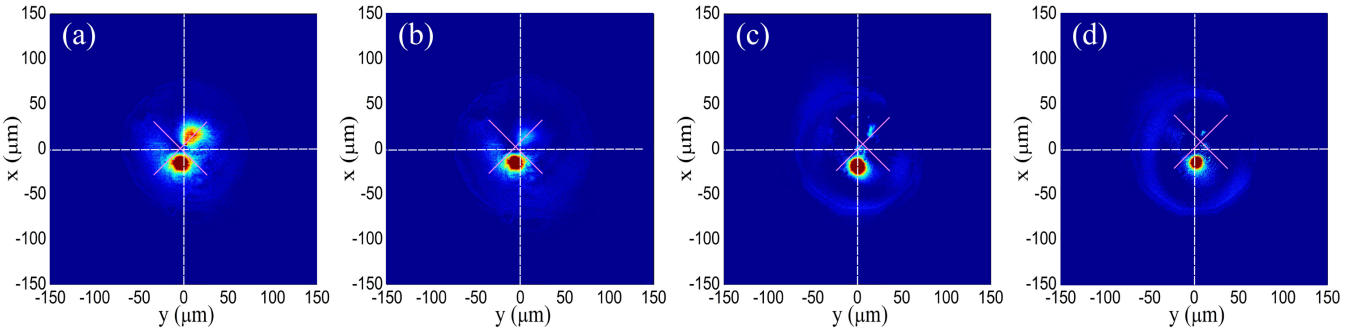

FIG. 3. Experimental images of the resultant transverse beam profiles at the output face of the cell obtained when the axis of the vortex and Gaussian beams are coincident (scheme B). Vortex beam intensity: 18 GW/cm^2. Gaussian beam intensity: (a) 0.3, (b) 0.8, (c) 1.4, and (d) 2 GW/cm^2. Cell length: 10 mm.

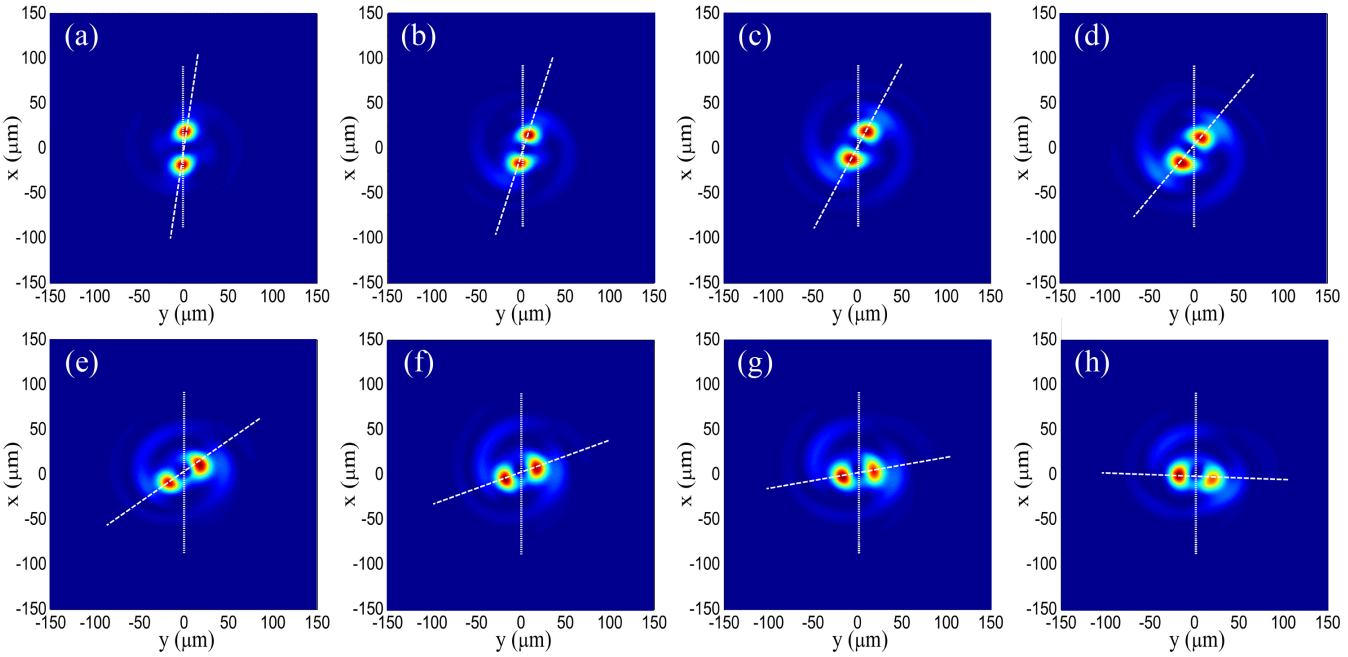

FIG. 4. Images of the emerging beam's profiles obtained from Eq. (1), following the input scheme of Fig. 1(b). $I_S = 15$ GW/cm^2 and I_C values of (a) 0, (b) 0.5, (c) 1, (d) 2.8, (e) 4.4, (f) 6.3, (g) 8.1, and (h) 9.3 GW/cm^2.

between the emerging beams is controlled by I_C which also controls the displacement of the vortex core. Nevertheless, the total power in the output face of the sample is conserved.

In order to compare the experimental results with a theoretical model, the propagation of both beams was described considering the contributions of the saturated refractive nonlinearity and the 3PA previously demonstrated for CS_2 at 532 nm, in the picosecond regime [20,22]. Based on these NL contributions, the propagation and interaction between the SB and the CB were described by a modified NL Schrödinger equation which assumes the form given by $i(\partial E_{in}/\partial z) + 1/(2n_0k)\Delta_\perp E_{in} = -[kaI_{in}^2/(1+b^2I_{in}^2) + i\gamma I_{in}^2/2]E_{in}$ [22], where E_{in} (I_{in}) corresponds to the incident field amplitude (peak intensity) expressed as a superposition of the vortex and Gaussian fields, $\Delta_\perp$ is the transverse Laplacian, z is the propagation direction, $k = 2\pi/\lambda$, λ is the laser wavelength, and n_0 is the linear refractive index. The first term of the right-hand side is due to the NL refractive behavior of CS_2 with the effective NL refractive index described by $n_{\text{eff}}^{(\text{NL})}(I) = aI^2/(1+b^2I^2)$, with $a = 6.3 \times 10^{-33}$ m^4/W^2 and $b = 2.3 \times 10^{-15}$ m^2/W [22]. The 3PA coefficient, $\gamma = 9.3 \times 10^{-26}$ m^3/W^2 reported in [22] was considered in the second term of the right-hand side.

In order to rescale the NL equation, we defined the variables, $X = x/w_0$, $Y = y/w_0$, $Z = z/L$, $U_{in} = E_{in}/E_r$, with $L = n_0kw_0^2$ and $E_r = (2bn_0c\varepsilon_0)^{-1/2}$, where w_0 is the initial beam waist of the SB, c is the speed of light in vacuum, and ε_0 the vacuum permittivity. After normalization, the modified nonlinear Schrödinger equation (NLSE) assumes the form

$$\frac{\partial U_{in}}{\partial Z} = \frac{i}{2}\left(\frac{\partial^2 U_{in}}{\partial X^2} + \frac{\partial^2 U_{in}}{\partial Y^2}\right) + i\frac{\eta|U_{in}|^4 U_{in}}{1+|U_{in}|^4} - \mu|U_{in}|^4 U_{in}, \tag{1}$$

with $\eta \equiv Lka/b^2$ and $\mu \equiv \gamma L/(2b^2)$. The incident intensity is related to the normalized field by $I_{in} = |U_{in}|^2/b$. Equation (1) is solved numerically by using the split-step compact finite-difference method [28]. The input beam profile in adimensional polar coordinates ($R = \sqrt{X^2+Y^2}$ and θ), considered for numerical simulations, has the form $U_{in}(R,\theta,z) = U_S \exp(-R^2 + i\theta)\tanh[w_0R/(2w_v)]\exp(i\Delta\phi) + U_C \exp[-(w_0^2/w_G^2)(R-d)^2]$, where U_S and U_C correspond to incident vortex (signal) and Gaussian (control) field amplitudes. d is the initial transverse distance between SB and CB, $\Delta\phi$ is the phase difference between the beams. w_0, w_v, and w_G are the waists of the Gaussian background, vortex core, and CB, respectively. Values of $L = 2.3$ mm, $\eta = 28$, $\mu = 3.3$, and $\Delta\phi = 0$ were used to model the beams' propagation in the 10-mm-long cell filled by CS_2.

Figure 4 shows numerical images of the emerging beams when scheme A is used, according to Fig. 1(b). Figure 4(a) shows the spontaneous azimuthal symmetry breaking of the SB when $I_s = 15$ GW/cm^2 and $I_C = 0$, in agreement with Fig. 2(a). Figures 4(b)–4(h) illustrate the control over the fragments' rotation obtained from Eq. (1) with $I_s = 15$ GW/cm^2 and 0.5 GW/cm^2 $\leqslant I_C \leqslant$ 9.3 GW/cm^2. The dashed lines indicate the angular positions of the fragments corresponding to Fig. 2.

Figure 5 shows the numerical results corresponding to scheme B, indicated in Fig. 1(c). The ETs between the emerging beams with 15%, 44%, 68%, and 92% efficiency were obtained for $I_s = 15$ GW/cm^2 and I_C values of 0.15, 0.75, 1.2, and 2.2 GW/cm^2, respectively. Figures 5(a)–5(d) reproduce the experimental results shown in Figs. 3(a)–3(d). Displacement of the vortex core, by varying the value of I_C, is observed in Fig. 5 corroborating our interpretation given above. The SB intensity used for the numerical calculations (15 GW/cm^2), slightly different from the experimental SB

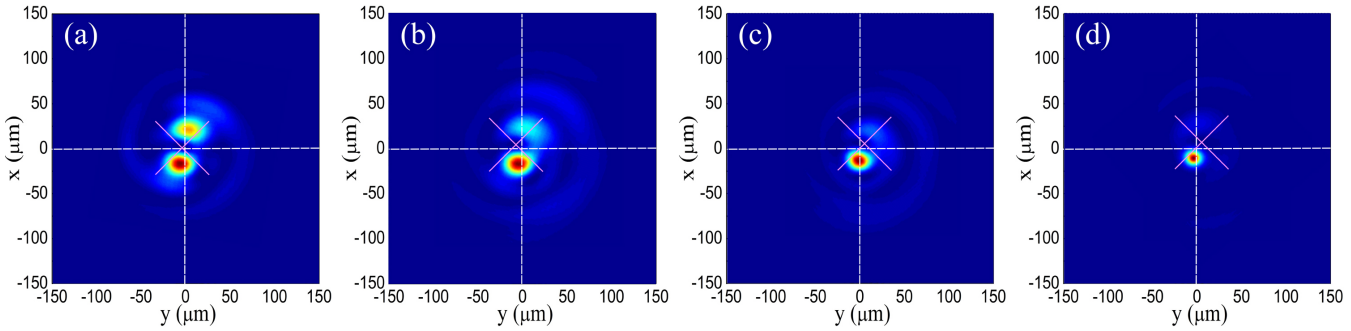

FIG. 5. Numerical output images of the fragments obtained from Eq. (1), following the scheme of Fig. 1(c). $I_S = 15$ GW/cm^2 and I_C values of (a) 0.15, (b) 0.75, (c) 1.2, and (d) 2.2 GW/cm^2.

intensity (18 GW/cm^2), was used to obtain very good agreement between the experimental and numerical results, for both schemes. The dashed lines correspond to the position of the vortex core when $I_C = 0$. The different I_C values used in the simulation and in the experiment are acceptable since fluctuations of ∼20% of the laser peak intensity are observed.

In order to get a qualitative understanding of the results we recall that in a nondissipative medium the emergent beams are fundamental solitons [14] that rotate along the tangent of the initial ring-type beam profile due to OAM conservation. After a certain propagation distance from the position where the vortex splits, conversion of rotational energy to centrifugal energy takes place and consequently, the fundamental solitons begin to move away from each other. In dissipative media, as in the case of CS_2, the fragments are not fundamental solitons because of the energy losses due to the 3PA. Then, the energy losses along the propagation dominate against the energy conversion process and the angular momentum of the fragments decreases with the relative distance between the fragments in the transverse plane being affected mainly by the linear diffraction. Therefore, the final position and distance between the two spots strongly depend on the characteristics of the input vortex beam and the nonlinearity of the medium. On the other hand, the control of rotation and the ET between the emerging fragments depend on the initial intensity, position, and radius of the *control beam*.

IV. SUMMARY AND CONCLUSIONS

In summary, we reported experiments that allow controlling the relative positions and energy of the two emerging beams produced due to the unstable OVS propagation in CS_2. A Gaussian beam overlapped with the optical vortex beam is used to control the behavior of the emerging fragments. Rotation of the emerging beams in the transverse plane by ∼90° and energy transfer among them with efficiency up to 92%, when the control beam has an intensity seven times smaller than the optical vortex beam, were observed. The experimental results were corroborated by numerical simulations based on a modified NLSE equation that describes the NL response of CS_2 under the present experimental conditions. The results shown here reveal an alternative and efficient approach for the design of all-optical modulators, where the output beams are strongly related because they are generated from a single initial beam.

ACKNOWLEDGMENTS

This work was supported by Brazilian agencies Conselho Nacional de Desenvolvimento Científico e Tecnológico (CNPq) and the Fundação de Amparo à Ciência e Tecnologia do Estado de Pernambuco (FACEPE). The work was performed in the framework of the National Institute of Photonics [INCT de Fotônica (INFO)] project and PRONEX/CNPq/FACEPE.

[1] O. Wada, New J. Phys. **6**, 183 (2004); A. Demircan, Sh. Amiranashvili, and G. Steinmeyer, Phys. Rev. Lett. **106**, 163901 (2011); J. Fatome, S. Pitois, P. Morin, and G. Millot, Opt. Express **18**, 15311 (2010).

[2] R. W. Boyd, *Nonlinear Optics* (Academic Press, New York, 2008); G. P. Agrawal, *Nonlinear Fiber Optics* (Academic Press, New York, 2001).

[3] M. Nakazawa, T. Yamamoto, and K. R. Tamura, Electron. Lett. **36**, 2027 (2000); M. Abb, P. Albella, J. Aizpurua, and O. L. Muskens, Nano Lett. **11**, 2457 (2011); D. Ballarini, M. De Giorgi, E. Cancellieri, R. Houdré, E. Giacobino, R. Cingolani, A. Bramati, G. Gigli, and D. Sanvitto, Nat. Commun. **4**, 1778 (2013); A. Abbasi and G. Morthier, IEEE J. Quantum Electron. **51**, 2200106 (2015); A. E. Willner, S. Khaleghi, M. R. Chitgarha, and O. F. Yilmaz, J. Lightwave Technol. **32**, 660 (2014).

[4] A. W. Snyder and F. Ladouceur, Opt. Photonics News **10**, 35 (1999); G. I. Stegeman and M. Segev, Science **286**, 1518 (1999); X. Liu, K. Beckwitt, and F. W. Wise, Phys. Rev. E **61**, R4722 (2000).

[5] Y.-D. Wu, Opt. Express **14**, 4005 (2006); Appl. Opt. **44**, 4144 (2005); Fiber Integr. Opt. **23**, 387 (2004).

[6] R. Y. Chiao, E. Garmire, and C. H. Townes, Phys. Rev. Lett. **13**, 479 (1964); A. Barthelemy, S. Maneuf, and C. Froehly, Opt. Commun. **55**, 201 (1985); J. S. Aitchison, A. M. Weiner, Y. Silberberg, M. K. Oliver, J. L. Jackel, D. E. Leaird, E. M. Vogel, and P. W. E. Smith, Opt. Lett. **15**, 471 (1990).

[7] P. L. Kelley, Phys. Rev. Lett. **15**, 1005 (1965); L. Bergé, Phys. Rep. **303**, 259 (1998).
[8] N. Akhmediev and J. M. Soto-Crespo, Phys. Rev. A **47**, 1358 (1993); V. Skarka, V. I. Berezhiani, and R. Miklaszewski, Phys. Rev. E **56**, 1080 (1997).
[9] E. L. Falcão-Filho, C. B. de Araújo, G. Boudebs, H. Leblond, and V. Skarka, Phys. Rev. Lett. **110**, 013901 (2013).
[10] A. S. Reyna, K. C. Jorge, and C. B. de Araújo, Phys. Rev. A **90**, 063835 (2014).
[11] Y. S. Kivshar and B. Luther-Davies, Phys. Rep. **298**, 81 (1998); Z. Chen, M. Segev, and D. N. Christodoulides, Rep. Prog. Phys. **75**, 086401 (2012).
[12] L. Allen, M. W. Beijersbergen, R. J. C. Spreeuw, and J. P. Woerdman, Phys. Rev. A **45**, 8185 (1992); A. S. Desyatnikov, Y. S. Kivshar, and L. Torner, Prog. Opt. **47**, 291 (2005); A. M. Amaral, E. L. Falcão-Filho, and C. B. de Araújo, Opt. Express **22**, 30315 (2014).
[13] G. A. Swartzlander, Jr. and C. T. Law, Phys. Rev. Lett. **69**, 2503 (1992); Y. S. Kivshar and G. P. Agrawal, *Optical Solitons: From Fibers to Photonic Crystals* (Academic Press, San Diego, CA, 2003).
[14] W. J. Firth and D. V. Skryabin, Phys. Rev. Lett. **79**, 2450 (1997); D. V. Skryabin and W. J. Firth, Phys. Rev. E **58**, 3916 (1998).
[15] Y. S. Kivshar and D. E. Pelinovsky, Phys. Rep. **331**, 117 (2000).
[16] L. T. Vuong, T. D. Grow, A. Ishaaya, A. L. Gaeta, G. W. 't Hooft, E. R. Eliel, and G. Fibich, Phys. Rev. Lett. **96**, 133901 (2006).
[17] C. Rotschild, O. Cohen, O. Manela, M. Segev, and T. Carmon, Phys. Rev. Lett. **95**, 213904 (2005); Y. V. Kartashov, V. A. Vysloukh, and L. Torner, *ibid.* **94**, 043902 (2005); Opt. Express **15**, 9378 (2007); A. I. Yakimenko, Y. A. Zaliznyak, and Y. Kivshar, Phys. Rev. E **71**, 065603 (2005); M. Quiroga-Teixeiro and H. Michinel, J. Opt. Soc. Am. B **14**, 2004 (1997); H. Michinel, J. Campo-Táboas, M. L. Quiroga-Teixeiro, J. R. Salgueiro, and R. García-Fernández, J. Opt. B: Quantum Semiclass. Opt. **3**, 314 (2001); I. Towers, A. V. Buryak, R. A. Sammut, and B. A. Malomed, Phys. Rev. E **63**, 055601 (2001); B. A. Malomed, L.-C. Crasovan, and D. Mihalache, Physica D **161**, 187 (2002); D. Mihalache, D. Mazilu, B. A. Malomed, and F. Lederer, Phys. Rev. E **69**, 066614 (2004).
[18] Z. Wu, Y. Zhang, C. Yuan, F. Wen, H. Zheng, Y. Zhang, and M. Xiao, Phys. Rev. A **88**, 063828 (2013).
[19] D. N. Neshev, T. J. Alexander, E. A. Ostrovskaya, Y. S. Kivshar, H. Martin, I. Makasyuk, and Z. Chen, Phys. Rev. Lett. **92**, 123903 (2004); J. W. Fleischer, G. Bartal, O. Cohen, O. Manela, M. Segev, J. Hudock, and D. N. Christodoulides, *ibid.* **92**, 123904 (2004).
[20] A. S. Reyna, G. Boudebs, B. A. Malomed, and C. B. de Araújo, arXiv:1511.06009 [Phys. Rev. A (to be published)].
[21] S.-M. Li, Y. Li, X.-L. Wang, L.-J. Kong, K. Lou, C. Tu, Y. Tian, and H.-T. Wang, Sci. Rep. **2**, 1007 (2012); D. V. Petrov, L. Torner, J. Martorell, R. Vilaseca, J. P. Torres, and C. Cojocaru, Opt. Lett. **23**, 1444 (1998); V. Tikhonenko, J. Christou, and B. Luther-Daves, J. Opt. Soc. Am. B **12**, 2046 (1995).
[22] V. Besse, H. Leblond, and G. Boudebs, Phys. Rev. A **89**, 043840 (2014).
[23] B. Luther-Davies, R. Powles, and V. Tikhonenko, Opt. Lett. **19**, 1816 (1994).
[24] S. Couris, M. Renard, O. Faucher, B. Lavorel, R. Chaux, E. Koudoumas, and X. Michaut, Chem. Phys. Lett. **369**, 318 (2003).
[25] A. S. Reyna and C. B. de Araújo, Opt. Express **23**, 7659 (2015).
[26] J. Christou, V. Tikhonenko, Y. S. Kivshar, and B. Luther-Davies, Opt. Lett. **21**, 1649 (1996).
[27] D. Rozas, C. T. Law, and G. A. Swartzlander, Jr., J. Opt. Soc. Am. B **14**, 3054 (1997).
[28] S. Wang and L. Zhang, Comput. Phys. Commun. **184**, 1511 (2013).